THE UNIVERSITY of EDINBURGH

Edinburgh Research Explorer

Targeted microbubbles carrying lipid-oil-nanodroplets for ultrasound-triggered delivery of the hydrophobic drug, Combretastatin A4

Citation for published version:
Charalambous, A, Mico, V, McVeigh, LE, Marston, G, Ingram, N, Volpato, M, Peyman, SA, McLaughlan, JR, Wierzbicki, A, Loadman, P, Bushby, RJ, Markham, AF, Evans, SD & Coletta, PL 2021, 'Targeted microbubbles carrying lipid-oil-nanodroplets for ultrasound-triggered delivery of the hydrophobic drug, Combretastatin A4', *Nanomedicine: Nanotechnology, Biology and Medicine*.
https://doi.org/10.1016/j.nano.2021.102401

Digital Object Identifier (DOI):
10.1016/j.nano.2021.102401

Link:
Link to publication record in Edinburgh Research Explorer

Document Version:
Peer reviewed version

Published In:
Nanomedicine: Nanotechnology, Biology and Medicine

General rights
Copyright for the publications made accessible via the Edinburgh Research Explorer is retained by the author(s) and / or other copyright owners and it is a condition of accessing these publications that users recognise and abide by the legal requirements associated with these rights.

Take down policy
The University of Edinburgh has made every reasonable effort to ensure that Edinburgh Research Explorer content complies with UK legislation. If you believe that the public display of this file breaches copyright please contact openaccess@ed.ac.uk providing details, and we will remove access to the work immediately and investigate your claim.

OPEN ACCESS

Download date: 06. May. 2023

Nanomedicine: Nanotechnology, Biology, and Medicine
xx (xxxx) xxx

nanomedicine
Nanotechnology, Biology, and Medicine

nanomedjournal.com

Graphical abstract

Nanomedicine: Nanotechnology, Biology, and Medicine xxx (2021) xxx–xxx

Targeted microbubbles carrying lipid-oil-nanodroplets for ultrasound-triggered delivery of the hydrophobic drug, Combretastatin A4

A Charalambous[a], V Mico[b], LE McVeigh[a], G Marston[a], N Ingram[a], M Volpato[a], SA Peyman[a,b], JR McLaughlan[c], A Wierzbicki[d], P Loadman[d], RJ Bushby[b,e], AF Markham[a], SD Evans[b], PL Coletta[a,*]

[a]*Leeds Institute of Medical Research, Wellcome Trust Brenner Building, St James's University. Hospital, Leeds, United Kingdom*
[b]*Molecular and Nanoscale Physics Group, School of Physics and Astronomy, University of Leeds, Leeds, United Kingdom*
[c]*School of Electronic and Electrical Engineering, University of Leeds, United Kingdom*
[d]*Institute of Cancer Therapeutics, University of Bradford, Bradford, United Kingdom*
[e]*School of Chemistry, University of Leeds, Leeds, United Kingdom*

A number of highly potent and promising drugs fail to reach the clinic due to poor-water solubility. Lipid-stabilized Oil Nanodroplets (LONDs) were produced specifically for the encapsulation of poorly-water soluble drugs such as the vascular disruptive agent Combretastatin A4 (CA4). Initial pre-clinical work with CA4 LONDs showed an accumulation of CA4 in tumor tissue. Attachment of CA4 LONDs to VEGFR2-targeted Microbubbles (MBs) permitted the controlled and ultrasound triggered release of CA4 in tumors, confirmed by a reduction in tumor perfusion post-treatment. The combination of low dose irinotecan with CA4 LONDs-MBs further enhanced the anti-tumor effects of both compounds

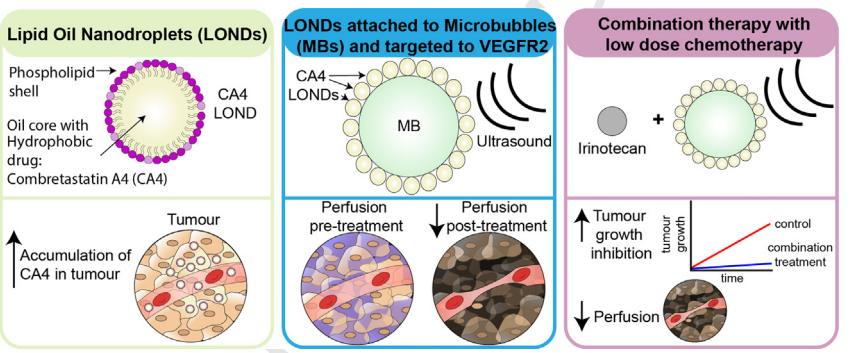

UNCORRECTED PROOF

Please cite this article as: Charalambous A., et al., Targeted microbubbles carrying lipid-oil-nanodroplets for ultrasound-triggered delivery of the hydrophobic drug, Combretastatin A4. *Nanomedicine: NBM* 2021;xx:0-11, https://doi.org/10.1016/j.nano.2021.102401

ELSEVIER
Nanomedicine: Nanotechnology, Biology, and Medicine
xx (xxxx) xxx
nanomedicine
Nanotechnology, Biology, and Medicine
nanomedjournal.com

Targeted microbubbles carrying lipid-oil-nanodroplets for ultrasound-triggered delivery of the hydrophobic drug, Combretastatin A4☆

A Charalambous[a], V Mico[b], LE McVeigh[a], G Marston[a], N Ingram[a], M Volpato[a], SA Peyman[a,b], JR McLaughlan[c], A Wierzbicki[d], P Loadman[d], RJ Bushby[b,e], AF Markham[a], SD Evans[b], PL Coletta[a,*]

[a]*Leeds Institute of Medical Research, Wellcome Trust Brenner Building, St James's University. Hospital, Leeds, United Kingdom*
[b]*Molecular and Nanoscale Physics Group, School of Physics and Astronomy, University of Leeds, Leeds, United Kingdom*
[c]*School of Electronic and Electrical Engineering, University of Leeds, United Kingdom*
[d]*Institute of Cancer Therapeutics, University of Bradford, Bradford, United Kingdom*
[e]*School of Chemistry, University of Leeds, Leeds, United Kingdom*

Revised 3 March 2021

Abstract

The hydrophobicity of a drug can be a major challenge in its development and prevents the clinical translation of highly potent anti-cancer agents. We have used a lipid-based nanoemulsion termed Lipid-Oil-Nanodroplets (LONDs) for the encapsulation and *in vivo* delivery of the poorly bioavailable Combretastatin A4 (CA4). Drug delivery with CA4 LONDs was assessed in a xenograft model of colorectal cancer. LC–MS/MS analysis revealed that CA4 LONDs, administered at a drug dose four times lower than drug control, achieved equivalent concentrations of CA4 intratumorally. We then attached CA4 LONDs to microbubbles (MBs) and targeted this construct to VEGFR2. A reduction in tumor perfusion was observed in CA4 LONDs-MBs treated tumors. A combination study with irinotecan demonstrated a greater reduction in tumor growth and perfusion ($P = 0.01$) compared to irinotecan alone. This study suggests that LONDs, either alone or attached to targeted MBs, have the potential to significantly enhance tumor-specific hydrophobic drug delivery.
© 2021 Published by Elsevier Inc.

Key words: Lipid-Oil-Nanodroplets (LONDs); Combretastatin A4; Microbubbles; Targeting; Ultrasound trigger

Poor drug physiochemical properties such as hydrophobicity are one of the main causes of drug failure during the early developmental stages. Approximately 40% of currently approved drugs and up to as many as 90% of drugs in the discovery pipeline exhibit poor aqueous solubility.[1] As a consequence, these compounds suffer from low bioavailability, often with rapid metabolism and excretion. The consequent need for higher dosing leads to poor safety and tolerability profiles.[1] Among hydrophobic agents with potential value in cancer treatment is the vascular disrupting agent (VDA), Combretastatin A4 (CA4). Unlike anti-angiogenic agents which target angiogenesis and prevent the development of new blood vessels, VDAs target the

Abbreviations: 5-FU, 5-fluorouracil; CA4, Combretastatin A4; CA4G, CA4 glucuronide; CA4P, CA4 phosphate; CEPs, circulating endothelial progenitor cells; CRC, colorectal cancer; EPR, enhanced permeability and retention; i.p., intraperitoneal; i.v., intravenous; ICAM-1, intracellular adhesion molecule-1; LOD, limit of detection; LONDs, Lipid-Oil-Nanodroplets; MBs, microbubbles; TGI, tumor growth inhibition; Tx, treatment; US, ultrasound; VDA, vascular disrupting agent; VEGFR2, vascular endothelial growth factor receptor 2

Disclosure of interest statement: None
Statement of funding: The work was funded by the Medical Research Council (grant number: MR/L01629X MRC Medical Bioinformatics Centre) and the EPSRC (grant number EP/P023266/1 Health Impact Partnership). EPSRC (EP/I000623/1, EP/K023845/1). Laura E. McVeigh was funded by an EPSRC PhD Studentship (EP/L504993/1).

* Corresponding author at: Leeds Institute of Medical Research, Wellcome Trust Brenner Building, St James's University. Hospital, Leeds, United Kingdom.
E-mail address: P.L.Coletta@leeds.ac.uk. (P.L. Coletta).

https://doi.org/10.1016/j.nano.2021.102401
1549-9634/© 2021 Published by Elsevier Inc.

UNCORRECTED PROOF

Please cite this article as: Charalambous A., et al., Targeted microbubbles carrying lipid-oil-nanodroplets for ultrasound-triggered delivery of the hydrophobic drug, Combretastatin A4. *Nanomedicine: NBM* 2021;xx:0-11, https://doi.org/10.1016/j.nano.2021.102401

already established tumor vasculature in the core of the tumor which are often resistant to conventional chemotherapy.[2] Numerous preclinical studies have shown that VDAs cause a significant reduction in tumor blood flow in the core of the tumor followed by secondary necrosis.[3–5] However, VDAs spare the rapidly proliferating cells of the tumor periphery, leaving behind a "viable rim" of cells which is a major cause of resistance and the reason for combination treatments with conventional chemotherapy.[6]

CA4 is a natural product originally isolated from the African tree *Combretum caffum*. It is a potent inhibitor of microtubule polymerization[7,8] binding near the colchicine binding site and preventing the "curved" to "straight" tubulin transition.[9] *In vitro*, CA4 causes complete disorganization of cytoskeletal microtubules in endothelial cells, which *in vivo* manifests as the rapid shutdown of tumor vasculature.[10,11] Due to its poor aqueous solubility, the prodrug CA4 phosphate (CA4P) has been developed.[12] Although CA4P improves the delivery of CA4, its use in clinical trials was compromised by unacceptable off-site toxicities.[13,14] An alternative route to improving solubility of hydrophobic compounds such as CA4 is to produce nano-formulations by using liposomes,[15] polymer based micelles[16] or nanoemulsions.[17,18]

Nanoparticles show excellent potential as drug-loaded carriers; however, some formulations suffer rapid clearance and/or nonspecific accumulation with drug release in healthy tissues.[19] It was assumed for many decades that a passive process known as the enhanced permeability and retention (EPR) effect was one of the main ways in which nanoparticles entered tumors leading to enhanced drug uptake.[19] However, recently, it has been shown using different mouse models, different types of human tumors, mathematical modeling and different imaging techniques that nanoparticles enter tumors using an active trans-endothelial process, suggesting that targeting of tumor endothelial cells may enhance uptake with nanoformulated drugs.[20]

MBs are intravascular ultrasound (US) contrast agents with diameters in the micrometer range, permitting their circulation in the bloodstream. MBs alone can be used in combination with US to increase drug-uptake and as drug delivery vehicles by directly incorporating drugs within MBs (within the shell) or by attaching payloads to the outside shell.[21,22] Further attachment of a targeting molecule on the surface of MBs can enable their binding at a specific disease site. For example, attachment of vascular endothelial growth factor receptor 2 (VEGFR2) antibodies has greatly enhanced the MB imaging of tumor vasculature.[23] *In vitro* and *in vivo* targeting of MBs to αvβ3 integrin or intracellular adhesion molecule-1 (ICAM-1) (both upregulated on tumor endothelium) has resulted in greater binding, with enhanced drug delivery to tumor endothelium compared to non-targeted MBs.[24,25]

VEGFR2-targeted MBs have been used to enhance delivery of attached liposomal payloads to tumors while reducing off-site toxicity.[22,26] An external US-trigger can induce localized MB oscillation and/or bursting leading to the induction of microstreams, shock waves and microjets.[27] These result in the release of the nano-formulated drugs, while simultaneously leading to the transient opening of pores in neighboring cell membranes, all potentially contributing to enhanced intratumoral drug delivery.[18,19]

We have previously developed Lipid-stabilized Oil Nanodroplets (LONDs) for the encapsulation and delivery of hydrophobic drugs such as CA4.[28] LONDs are formed by a two-step high-pressure homogenization process and range between 100 and 300 nm in diameter. The short chain triglyceride tripropionin was used as the oil core, having a water solubility of 0.003 g/L at 37 °C.[29] LONDs are stable for over six weeks when stored at 4 °C. Under physiological conditions they exhibit minimal changes in size over this period.[28] CA4 was successfully encapsulated in tripropionin LONDs and showed cellular uptake and release of CA4 *in vitro* as evidenced by the disruption of microtubules.[28]

In this study, *in vivo* biodistribution and intratumoral delivery of CA4 with CA4 LONDs and VEGFR2 targeted CA4 LONDs-MBs (Figure 1) were assessed using a mouse model of human colorectal cancer (CRC). The combined delivery of CA4 LONDs-MBs with the chemotherapeutic agent irinotecan was also evaluated *in vivo* and showed that low doses of CA4 drug delivered in this way enhanced tumor responses.

Methods

All experimental details can be found in the Supplementary Material.

Cell lines

SW480 cells were used in this study.

CA4 LOND production and characterization

Tripropionin LONDs encapsulating CA4 were produced by a two-step high-pressure homogenization described previously.[28]

CA4 LONDs-MBs microfluidic production and characterization

CA4 LOND-MBs were produced in a microfluidic device using a two-step process. The design of the microchip had a flow-focusing region for MB production using a microspray regime,[30] followed by a serpentine to allow for slower mixing of MBs with neutravidin functionalized CA4 LONDs (approximately 1.14 s[31]) (Supplementary Figure S1). MB-LONDs were characterized in terms of size and concentration. Based on these data, neutravidin VEGFR2 antibody (eBiosciences, UK) was added to the MBs at 0.1 μg per 10^7 MBs.

Mouse models

Local ethical approval was obtained and all experiments were undertaken in accordance with the UK Animals (Scientific Procedures) Act 1986. CD-1® and BALB/c nude mice were bred in-house under license from Charles River Laboratories (Wilmington, MA, USA) and maintained in specific-pathogen-free conditions in individually ventilated cages with free access to food and water. SW480 cells were used to form xenografts.

Tumor volume measurements

Tumor xenografts were imaged using a VisualSonics Vevo 770 high-frequency ultrasound system (Fujifilm VisualSonics

UNCORRECTED PROOF

ARTICLE IN PRESS

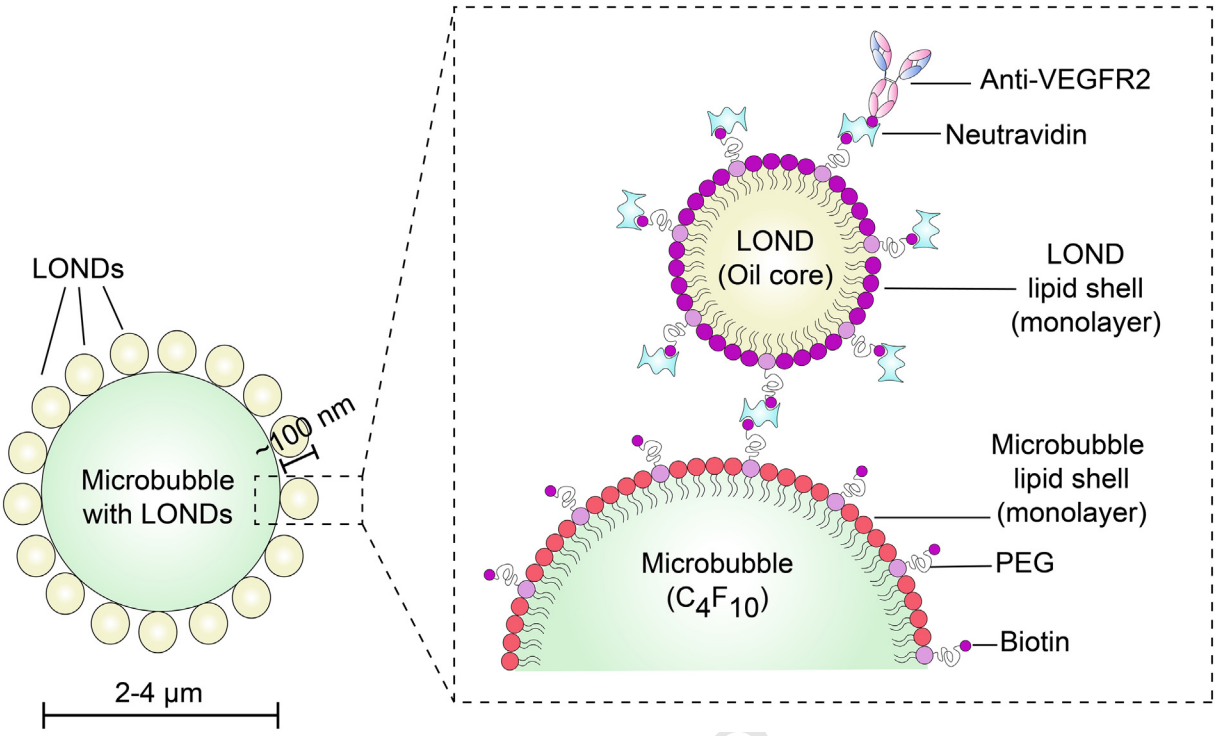

Figure 1. CA4 LONDs-MB schematic. The CA4 LONDs-MB construct consists of a lipid/PEG coated MB (light green representing the gas C_4F_{10} core with red shell) covalently conjugated (through biotin/neutravidin interactions) to a layer of LONDs (yellow with purple shell) encapsulating CA4 (dissolved in oil). The construct also carries anti-VEGFR2 antibodies to promote tumor specific delivery by allowing accumulation in tumor vasculature where VEGFR2 is more prevalent than in normal vasculature.

Inc., Ontario, Canada) equipped with 40 MHz (RM-704) and 25 MHz (RM-710B) transducers as previously described.[32,33]

Determination of vascular perfusion using the perfusion marker Hoechst 33342

Tumor perfusion was assessed by uptake of Hoechst 33342, a DNA binding dye that when left in the circulation for 1 min, stains the endothelial cells of blood vessels perfused at the time of injection.[34] Tumors were also stained with a primary antibody for CD31, visualized using an appropriate secondary antibody and imaged using a Zeiss Axioimager Z1 fluorescence microscope with AxioVision software (Carl Zeiss Microscopy, USA). Perfusion was scored using a semi-quantitative scoring system to define none (score 0), weak (score 1), moderate (score 2) and high (score 3) intensity of Hoechst 33342 fluorescent staining by two independent observers blinded to the treatment groups. Representative images for the perfusion scoring are shown in Supplementary Figure S2 for each data set. Data set 1 was used to score images represented in Figure 4 and data set 2 was used to score images represented in Figure 5 of the results section.

Liquid chromatography–tandem mass spectrometry (LC–MS/MS) for CA4, irinotecan, SN38 and SN38G detection

For the quantification of CA4 loading in LONDs, CA4 LONDs-MBs preparations and tissue samples, LC–MS/MS was used. Detection of irinotecan, SN38 and SN38G was performed following the method of Ingram et al 2020. The MRM setting for irinotecan, SN38 and SN38G is shown in Supplementary Table S1.

Table 1
LOND characterization: The mean diameter of LONDs and concentration were measured by DLS and NanoSight, respectively. The mean and standard deviation (SD) were calculated. CA4 loading in LONDs was measured by LC–MS/MS.

CA4 LOND preparation no.	CA4 LONDs concentration ($\times 10^{14}$/mL)	Mean diameter (nm)	CA4 concentration (mg/mL)
1	1.2	89	1.3
2	1.7	87	0.7
3	2	104	0.9
Mean	1.6	93	1
SD	0.4	10	0.3

Results

CA4 LOND characterization and in vivo biodistribution

CA4 LONDs were produced and physically characterized prior to *in vivo* delivery with LC–MS/MS being used to quantitate CA4 loading (Table 1). The mean diameter of three preparations of LONDs was 93 ± 10 nm as measured by DLS; the diameter was confirmed by particle tracking (NanoSight) which also calculated the concentration at 1.6 (± 0.4) × 10^{14} LONDs/mL. The mean CA4 loading from the three preparations was 1.0 ± 0.3 mg/mL measured by LC–MS/MS. The extraction efficiencies and limit of detection (LOD) of CA4 for the specifically designed LC–MS/MS method are shown in Supplementary Figure S3.

UNCORRECTED

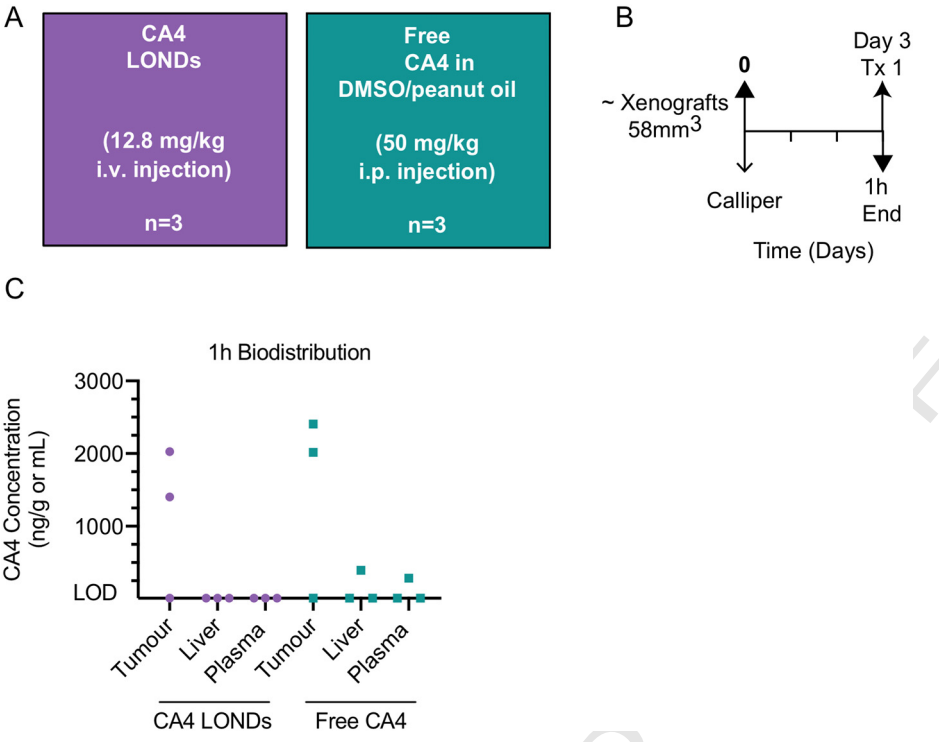

Figure 2. *In vivo* biodistribution of CA4 1 h post treatment with CA4 LONDs. **(A)** Treatment groups, doses used and delivery route are shown in brackets (n = number of mice per group). **(B)** Schematic of the treatment (Tx) schedule. Day 0 is the pre-treatment day where the mean (± SD) starting tumor volumes and mouse weights for each group were 53 (± 63) mm^3 and 33 (± 4) g for CA4 LONDs and 64 (± 22) mm^3 and 33 (± 4) g for free CA4. **(C)** CA4 concentrations in tumor, liver and plasma tissue 1 h post treatment with CA4 LONDs (12.8 mg/kg) and free CA4 (50 mg/kg). Limit of detection (LOD) for CA4 was 10 ng/mL.

To assess if drug delivery with CA4 LONDs altered the biodistribution of CA4, mice bearing SW480 human CRC xenografts were given a single treatment (preparation 1, Table 1) which equated to a dose of 12.8 mg/kg. Free CA4 dissolved in a combination of DMSO/peanut oil at 50 mg/kg (the standard dose in preclinical trials[10]) delivered intraperitoneally (i.p.) was used as a control (Figure 2, *A* and *B*). The concentration of CA4 in tumor, liver and plasma 1 h post treatment was determined using LC–MS/MS (Figure 2, *C*). CA4 was only detected in tumors (2/3) from the CA4 LONDs group, being below the LOD in liver and plasma while in the free CA4 group, CA4 was detected in tumors (2/3), in 1/3 liver and 1/3 plasma samples.

The main metabolite of CA4, CA4 glucuronide (CA4G) was also detected but not quantifiably (due to the lack of appropriate standards) in the plasma, liver and tumor from the free CA4 group and liver only from the CA4 LONDs group (Supplementary Table S2). The CA4G data suggest that delivery of free CA4 leads to its rapid metabolism to CA4G. While the detection of CA4G in the tumor samples suggested that CA4 was directly converted to CA4G intratumorally. However, it should be noted that due to the intraperitoneal delivery route of free CA4, CA4 may have undergone hepatic metabolism before entering the bloodstream. As CA4G was not detected in tumor samples from the CA4 LOND group this suggests that either CA4 is still encapsulated in the LONDs and unavailable for metabolism or encapsulated CA4 is potentially being released slowly into the tumor from the LONDs and the levels of CA4G following metabolism are below the LOD.

Nevertheless, these results confirmed that drug delivery to tumors of CA4 in both free and LOND encapsulated forms was possible and also showed that tumors from both groups were exposed to similar concentrations of CA4 even though the amount of CA4 in the LONDs was four times lower than free CA4.

Effect of CA4 LONDs on tumor growth following multiple treatments

As CA4 LONDs successfully delivered CA4 to tumor tissues, the potential of CA4 LONDs to cause tumor growth inhibition was assessed. Mice bearing SW480 CRC xenografts received three treatments (Tx) of CA4 LONDs (preparation 2, Table 1) or free CA4 dissolved in a combination of DMSO/peanut oil or vehicle control DMSO/peanut oil. CA4 LONDs and free CA4 were administered at a low dose of 3 mg/kg as using higher doses was not sustainable with multiple treatments (Figure 3, *A* and *B*). CA4 LONDs did not significantly delay the growth of tumors ($P = 0.8$). In contrast, free CA4 significantly inhibited tumor growth at day 3 compared to vehicle ($P = 0.01$) and CA4 LONDs ($P = 0.04$) (Figure 3, *C*). The % tumor growth inhibition (%TGI)[35] compared to vehicle (% TGI = 1 – (treated final – treated day 0)/(control final – control day 0)) was 17.5% for CA4 LONDs and 19.3% for free CA4. Tumor masses were lower in groups treated with CA4 LONDs and free CA4, while a modest increase in tumor doubling time was also observed in groups treated with CA4 LONDs and free CA4. However, these did not

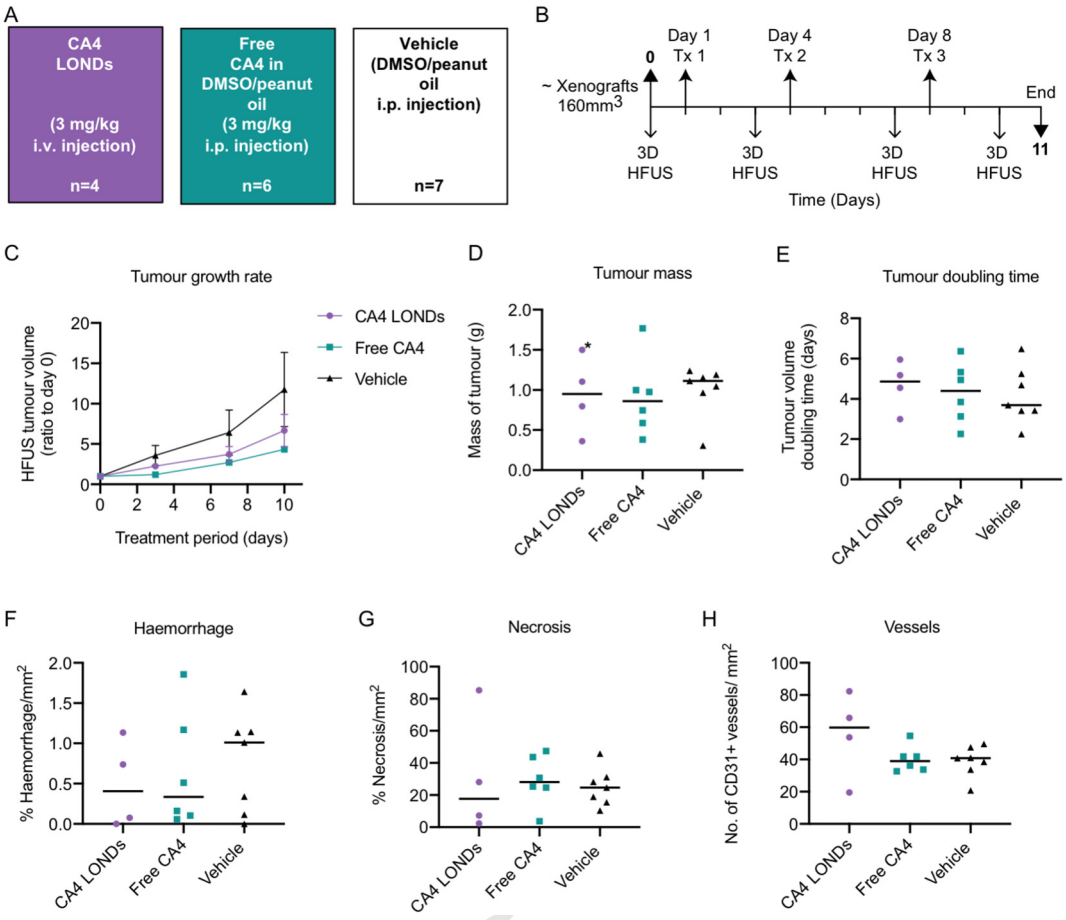

Figure 3. Tumor pharmacodynamic response to CA4 LONDs. **(A)** Treatment groups, doses and delivery route used are shown in brackets (n = number of mice per group). **(B)** Schematic of the treatment (Tx) schedule and 3D high frequency ultrasound (HFUS) imaging. Day 0 is the pre-treatment day where the mean (± SD) starting tumor volumes and mouse weights for each group were 147 (± 89) mm^3 and 21 (± 1) g for CA4 LONDs, 178 (± 89) mm^3 and 20 (± 1) g for free CA4 and 157 (± 129) mm^3 and 21 (± 3) g for vehicle which were not statistically significantly different at this time point. **(C)** Tumor volumes were measured by HFUS and the ratio to day 0 pre-treatment was plotted. Tumor growth rate was significantly inhibited at day 3 in the free CA4 group compared to vehicle (P = 0.01) and CA4 LONDs (P = 0.04). Mann–Whitney U test, two-tailed. Data represent the mean ± SEM. **(D)** Tumor mass in grams; * calculated mass based on the HFUS measurements at day 10 due to not measuring the weight at the time. **(E)** Tumor doubling time (days) was derived by fitting the tumor growth curve per mouse to an exponential growth curve. **(F)** % hemorrhage per mm^2 of tumor. **(G)** % necrosis per mm^2 of tumor. **(H)** Number of vessels per mm^2 of tumor was also manually counted. Horizontal lines ( ) represent the median in **D**-**H**.

reach statistical significance when compared to the vehicle DMSO/peanut oil (Figure 3, *D* and *E*).

Tumor response was further assessed by determining the % hemorrhage and necrosis in tumor tissue (Figure 3, *F* and *G*). CA4 LONDs and free CA4 did not appear to cause any treatment associated hemorrhage as the highest median % hemorrhage was observed in the vehicle group, pointing towards inherently leaky tumor vasculature (Figure 3, *F*). Despite extensive necrosis in 1/4 tumors treated with CA4 LONDs, the % necrosis was not significantly different from free CA4 and vehicle treated tumors (Figure 3, *G*). Treatment with CA4 LONDs and free CA4 did not significantly alter the number of CD31+ blood vessels compared to the vehicle (Figure 3, *H*).

Production and evaluation of targeted, ultrasound-triggered CA4 LONDs-MBs

Although CA4 LONDs were capable of delivering drug to tumors, the low doses encapsulated and delivered failed to significantly inhibit tumor growth. To enhance LOND drug delivery, we engineered MBs to carry LONDs. A preliminary study was conducted following the successful production of VEGFR2-targeted CA4 LONDs-MBs to assess the delivery of CA4 using the LOND-MB-construct by detecting changes in tumor perfusion.

The MB concentration, diameter and CA4 loading of the CA4 LONDs-MBs were 8×10^6/mL, 2.6 ± 1.5 μm and 0.0001 mg/mL measured by optical imaging and LC–MS/MS, respectively. 0.0001 mg/mL of CA4 is the concentration limit for the construct due to the dilutions involved during the two-step production process; therefore, 0.001 mg/kg was the highest dose that could be delivered. SW480 CRC xenograft-bearing mice were injected intravenously with CA4 LONDs-MBs at a concentration of 0.001 mg/kg or CA4P at 50 mg/kg or vehicle (PBS) (Figure 4, *A* and *B*). CA4P was used as the drug control to enable the same intravenous delivery route as CA4 LONDs-MBs and at 50 mg/kg to act as a positive control as previous studies

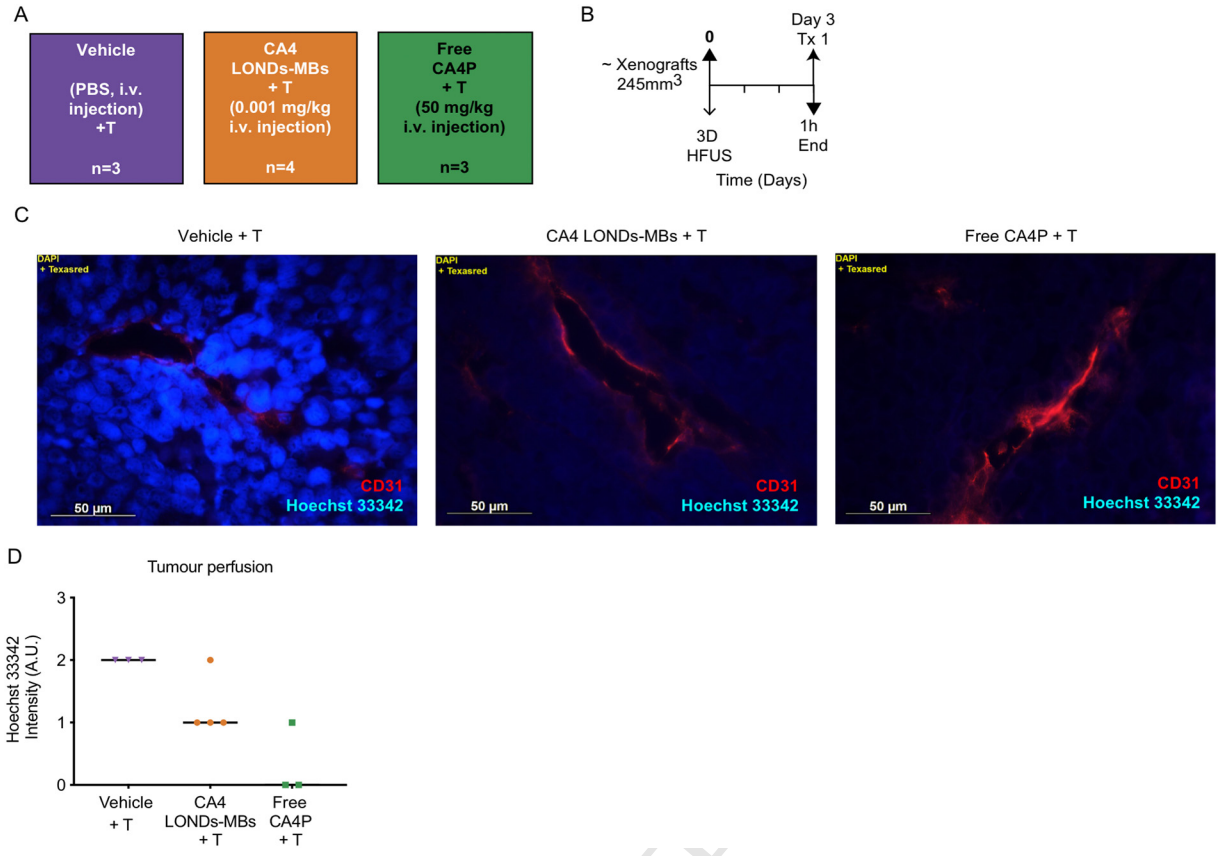

Figure 4. CA4 LONDs-MBs *in vivo* evaluation of tumor delivery and vascular shutdown following a single treatment. **(A)** Treatment groups, doses used and the number of mice per group (n). All groups were exposed to an US trigger (+T). **(B)** Schematic of the treatment (Tx) schedule and 3D high frequency ultrasound (HF-US) imaging. Day 0 is the pre-treatment day where the mean (± SD) starting tumor volumes for each group were 248 (± 79) mm^3 for CA4 LONDs-MBs, 273 (± 147) mm^3 for CA4P and 224 (± 242) mm^3 for vehicle; these were not statistically significantly different at this time point. **(C)** Representative fluorescent images of tumor sections showing perfusion in the tumor core stained with Hoechst 33342 *in situ* (blue) and CD31 vessels stained *ex vivo* (red). Scale bars indicate 50 µm. **(D)** Hoechst 33342 intensity scoring used to score perfusion (see Supplementary Figure S2 for scoring index). The data represent the median and error bars the interquartile range. Significance was calculated using a Mann–Whitney *U* test, two-tailed. A.U. arbitrary units. Horizontal line ( ) represents the median value.

UNCORRECTED

have shown a reduction in perfusion at concentrations of 50 mg/kg or above.[3,10,36] A low frequency, high amplitude US pulse was applied at the tumor site using a specifically designed custom-built single element US system (UARP) 4 min post-MB injection. All groups were exposed to a 5 s US trigger (+T). This was a 10 µs tone burst US pulse, with a peak negative pressure of 260 kPa and 1 kHz pulse repetition frequency (PRF), using a 2.2 MHz transducer designed to destroy the MBs *in situ*.

Tumor morphology at 1 h post treatment with CA4 LONDs-MBs or free CA4P was similar to vehicle treated tumors (data not shown). Most of the tumor was viable with some areas of hemorrhage present to the same extent as the vehicle group. Assessment of perfusion using Hoechst 33342 was adopted as a surrogate biomarker of tumor response, since quantitation of tumor necrosis, hemorrhage, blood vessel number and tumor volume was not sufficiently sensitive to detect any very early tumor responses to CA4 LOND therapy.

Perfusion in the tumor core was reduced in treated groups compared to vehicle (Figure 4, *C*). Perfusion in the tumor periphery was not reduced in the treated groups compared to vehicle (data not shown), suggesting that the tumor core was more susceptible to the effects of CA4. Although apparent differences in perfusion were observed between the groups, semi-quantitative analysis failed to show any statistically significant differences between them ($P = 0.1$) (Figure 4, *D*). Despite this, the fluorescent images showed a marked reduction in perfusion, strongly suggesting the successful uptake and/or release of CA4 intratumorally from the CA4 LONDs-MBs construct.

Combination therapy using low dose irinotecan and US triggered targeted CA4 LONDs-MBs

The results with CA4 LONDs-MBs showed evidence of CA4 uptake/release intratumorally, as a reduction in perfusion was observed and this was achieved using a very low dose of CA4 (0.001 mg/kg). As the delivery of CA4 alone is considered unlikely to be curative,[37–39] CA4 LONDs-MBs were combined with irinotecan to further enhance the anti-tumor activity achieved with CA4. Irinotecan is a prodrug requiring conversion

by cellular carboxylesterases to its active metabolite SN38, a topoisomerase I inhibitor used in the treatment of CRC and liver metastases.[40] A low and frequent dosing schedule (metronomic) was chosen since reports have shown that frequent lower doses of CA4P are more effective at sustaining its anti-tumor effects.[41] Irinotecan administered using a metronomic schedule has also shown enhanced efficacy, potentially by exerting additional anti-angiogenic effects.[40,42]

There is conflicting evidence regarding the timing and sequence of administration of CA4P when used in combination therapy. Theoretically the greatest anti-tumor activity should be observed when CA4P is administered after or concurrently with the combination agent, as potential changes to the tumor microenvironment induced by CA4P may hinder partner drug uptake.[43–46] Irinotecan (10 mg/kg) was administered 1 h prior to CA4 LONDs-MBs (0.001 mg/kg) or CA4P (0.001 mg/kg) to treat SW480 human CRC xenografts (Figure 5, *A*). CA4 LONDs-MBs and CA4P were administered at the same concentration to investigate if the targeted, triggered delivery of CA4 using the LOND-MB construct had a greater effect on tumor growth compared to delivering free drug systemically. Administrating irinotecan 1 h prior to any other treatment allows for the active metabolite of irinotecan, SN38 to reach its peak conversion in the blood.[47]

Mice received five treatments in total over three weeks (Figure 5, *B*). The mean concentration, diameter and CA4 loading in CA4 LONDs-MBs used for the five treatments were 3.5×10^7 MBs/mL, 4 ± 0.3 μm and 0.0001 ± 0.00006 mg/mL respectively (Supplementary Table S3).

Tumor growth was inhibited in both combination groups with irinotecan and CA4 LONDs-MBs or CA4P. Irinotecan + CA4 LONDs-MBs significantly inhibited the growth of tumors by day 11 compared to vehicle control (PBS) ($P = 0.05$) (Figure 5, *C*). In contrast the combination therapy with irinotecan and CA4P significantly inhibited the growth of tumors from day 7 onwards when compared to vehicle ($P = 0.01$, $P = 0.02$ and $P = 0.04$) (Figure 5, *C*). By day 14 after the fourth treatment, tumor growth was also inhibited in the irinotecan + CA4P group compared to irinotecan alone ($P = 0.04$) (Figure 5, *C*). The %TGI compared to vehicle was 22.9% for irinotecan only, 88.5% for irinotecan and CA4P and 47.8% for irinotecan and CA4 LONDs-MBs. Compared to irinotecan the %TGI was 85.1% for irinotecan and CA4P and 32.2% for irinotecan and CA4 LONDs-MBs.

Tumors in all treatment groups were smaller in mass than vehicle controls. However, only tumors in the irinotecan + CA4P group reached statistical significance when compared to vehicle ($P = 0.02$) (Figure 5, *D*). Tumor doubling times were not significantly increased in the irinotecan and CA4P group compared to vehicle (Supplementary Figure S4). Tumor regression was also observed in all treatment groups (Supplementary Figure S4). Body weight was monitored throughout the study with only very mild body weight loss observed in the irinotecan only group after the initial treatment (before recovering by treatment three) (Supplementary Figure S5).

To determine potential mechanisms by which the combination therapy of irinotecan and CA4 LONDs-MBs might be enhancing tumor growth inhibition, tumor perfusion was assessed. Tumor sections from the vehicle group and the irinotecan only group appeared to be well perfused when compared to the combination groups of irinotecan + CA4 LONDs-MBs or CA4P (Figure 5, *E*). Semi-quantitative assessment of the fluorescent images demonstrated that tumor perfusion was significantly reduced in the irinotecan + CA4 LONDs-MBs combination group compared to vehicle control ($P = 0.02$) (Figure 5, *F*). No statistically significant difference was observed when comparing irinotecan + CA4 LONDs-MBs to irinotecan alone; this was potentially due to irinotecan causing necrosis and a subsequent reduction in overall tumor perfusion following the five treatments.

Tumor, tissue drug biodistribution and metabolism following multiple treatments

Tumor and tissue biodistribution of irinotecan and its metabolites was assessed to determine if the CA4 LOND MB or free CA4 combinations altered its pharmacokinetic response. The concentrations of irinotecan and its active and inactive metabolites, SN38 and SN38G respectively, were determined by LC–MS/MS 1 h post final treatment in tumors, plasma, liver, colon (Figure 6) and in spleen, kidney, lung and heart tissues (Supplementary Figure S6).

The presence of CA4 (in the LONDs-MBs construct) or free CA4P did not appear to alter tumor metabolism of irinotecan to SN38 and SN38G (Figure 6, *A*). However, it potentially altered the ability of irinotecan to enter the tumor following five treatments as the concentration of irinotecan was significantly higher in the irinotecan only group compared to irinotecan + CA4P ($P = 0.005$) and irinotecan + CA4 LONDs-MBs ($P = 0.002$). This suggested that following five treatments in the combination groups the vasculature of the tumors was significantly altered as observed in Figure 5, *F* hindering the entry of irinotecan. Plasma and liver concentrations of irinotecan, SN38 and SN38G (Figure 6, *B* and *C*) were not altered by the combination. Interestingly, the metabolism of irinotecan to SN38 and SN38G in colon was much more variable compared to the other organs in all groups (Figure 6, *D*) (Supplementary Figure S6).

Discussion

The issues of drug solubility, limited bioavailability and toxicity have prompted the development of a plethora of nano-formulated drugs with various characteristics and potential structural modifications. In the present study we have demonstrated that LONDs can be used for the encapsulation and *in vivo* delivery of the hydrophobic drug, CA4. CA4 has been previously incorporated in a number of liposomal formulations.[48–51] One potential advantage of our LONDs compared to liposomes is that hydrophobic drugs (such as CA4) are encapsulated in the core of the particle rather than incorporated in the lipid bilayer of the liposome. Incorporation into the lipid bilayer, although widely used for hydrophobic drugs, has several limitations including restrictions in drug loading and the potential for drug leakage due to destabilization of the membrane from changes in the phase transition temperature.[52]

The data presented in this study showed that CA4 LONDs administered *in vivo* at a dose four times lower than free CA4,

UNCORRECTED PROOF

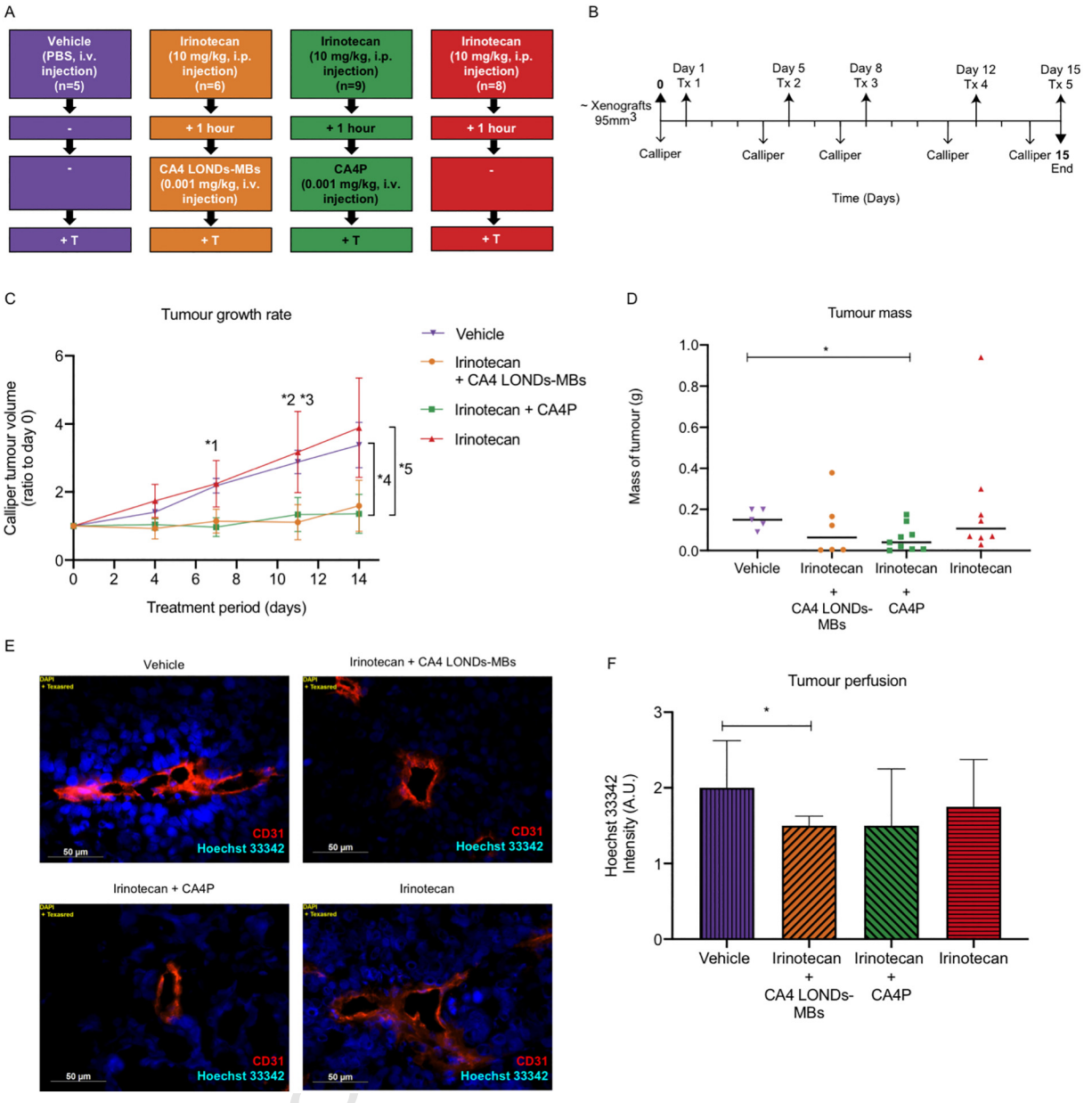

Figure 5. Combination therapy using irinotecan and CA4 LONDs-MBs to treat CRC. **(A)** Treatment groups, doses used and delivery route (n = number of mice per group). All groups were exposed to an US trigger (+T). **(B)** Treatment schedule. Mice received five treatments (Tx) in total over three weeks. 1 h after the fifth and final treatment tumors were excised for *ex vivo* analysis. Day 0 is the pre-treatment day where the mean (± SD) starting tumor volumes for each group were 99 (± 46) mm^3 for irinotecan + CA4 LONDs-MBs, 95 (± 70) mm^3 for irinotecan + CA4P, 91 (± 46) mm^3 for irinotecan only and 97 (± 26) mm^3 for vehicle; these were not statistically significantly different at this time point. **(C)** Tumor growth rate is plotted. Data represent the mean ± SEM; P values were determined by Mann–Whitney U test, two tailed. *1 $P = 0.01$ (irinotecan + CA4P *vs* vehicle), *2 $P = 0.02$ (irinotecan + CA4P *vs* vehicle), *3 $P = 0.05$ (irinotecan + CA4 LONDs-MBs *vs* vehicle), *4 $P = 0.04$ (irinotecan + CA4P *vs* vehicle), *5 $P = 0.04$ (irinotecan + CA4P *vs* irinotecan). **(D)** Tumor mass in grams on excision. Tumors were significantly smaller in the irinotecan + CA4P group compared to PBS ($P = 0.02$). Horizontal line ( ) represent the median. **(E)** Representative fluorescent images of tumor sections showing tumor perfusion in the tumor core stained with Hoechst 33342 *in situ* (blue) and CD31 vessels (red) stained *ex vivo*. Scale bars indicate 50 µm. **(F)** Hoechst 33342 intensity scoring used to score perfusion. A statistically significant difference ($P = 0.02$) was observed between vehicle and irinotecan + CA4 LONDs-MBs. The data represent the median score from two independent blinded assessors and the error bars denote the interquartile range. Significance was calculated using a Mann–Whitney U test, two-tailed.

delivered a similar concentration of CA4 intratumorally (~1000 ng/g) with none detected (or below the LOD) in the liver or plasma 1 h post treatment. In contrast, CA4 was present in the liver and plasma samples from the free CA4 group. It was therefore concluded that CA4 LONDs were more effective at delivering CA4 to the tumor, without the need for high circulating concentrations of free drug. Wang et al investigated the *in vivo* tumor and tissue biodistribution of CA4/methotrexate co-loaded nanoparticles delivered i.v. at a CA4 dose of 15 mg/kg and found tumor concentrations consistent with our results.[53]

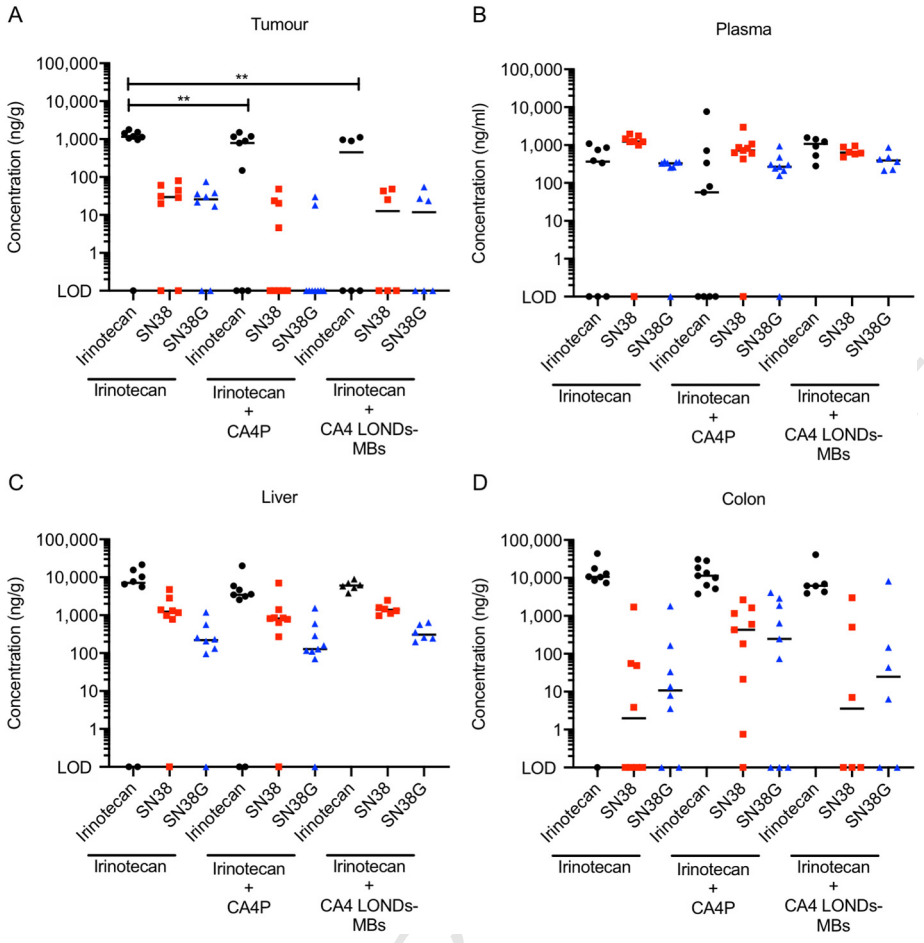

Figure 6. Tumor and tissue biodistribution of CA4, irinotecan and its active and inactive metabolites SN38 and SN38G 1 h post-treatment. For treatment groups and dosing schedule, see Figure 5, *A* and *B*. The concentrations of irinotecan, SN38 and SN38G per gram of tissue were determined in **(A)** tumor, **(B)** plasma, **(C)** liver and **(D)** colon. Two-way ANOVA followed by Holm–Sidak's multiple comparisons test showed that a significantly higher concentration of irinotecan was observed in the irinotecan only group compared to irinotecan + CA4P ($P = 0.005$) and irinotecan + CA4 LONDs-MBs ($P = 0.002$). Horizontal line ( ) represents the median value. LOD for irinotecan, SN38 and SN38G was 10 pg/L.

Numerous pre-clinical studies have shown that the effects of a single treatment with CA4 or CA4P on the growth of tumors are very limited with modest growth delays only observed at doses higher than 100 mg/kg. This is mainly attributed to the viable rim remaining post treatment.[38] Therefore in order to obtain a better therapeutic response with CA4, multiple dosing regimens are used.[41] The timings between treatments in our study were over 24 h, as a longer retention and prolonged exposure in the tumor were anticipated with CA4 LONDs, due to the encapsulation as opposed to free drug. However, CA4 LONDs caused a modest but statistically insignificant tumor growth inhibition (Figure 3). This was potentially due to the timings between treatments as tumors generally recover from the effects of CA4 24 and 48 h post treatment.[41,45,54,55] In contrast, administrating free CA4 at 3 mg/kg every other day for a total of five treatments has been shown to significantly inhibit growth of hepatocellular carcinoma.[53]

The combination of nanoparticles with targeted MBs and US has been shown to enhance the efficacy of drugs by increasing the circulation times and improving drug accumulation in tumor cells.[26,27] In this study, CA4 LONDs were attached to VEGFR2-targeted MBs to enable US-triggered delivery. Tumor perfusion as assessed by Hoechst 33342 (a perfusion marker) indicated successful delivery of CA4 from the LOND-MB construct as a clear reduction in tumor core perfusion was observed, with changes to the tumor periphery, consistent with previous reports using CA4P.[3,38,56] A greater reduction in perfusion was observed in the free CA4P group (50 mg/kg) compared to CA4 LONDs-MBs (0.001 mg/kg) most likely due to the large difference in dose. A reduction in perfusion has previously been shown to be dose-dependent with CA4[36] and lack of tumor response at the tumor periphery has been widely reported in animal models.[3,4,57] This has been attributed to the differences in vasculature between tumor core and its periphery. Tumor vessels in the periphery are more mature; they have a greater investiture of smooth muscle cells and have lower levels of hypoxia, as they are close to 'normal' vessels and have higher expression of VEGF.[58]

To further improve the effectiveness of US-triggered, VEGFR2-targeted CA4 LONDs-MBs these were combined

ARTICLE IN PRESS

with the chemotherapeutic agent irinotecan. This resulted in a significant tumor growth inhibition when irinotecan was given with either CA4 LONDs-MBs or CA4P demonstrating that longitudinally CA4 LONDs-MBs were as effective at delivering a hydrophobic drug such as CA4 when compared to CA4P. The combination of irinotecan and CA4P also significantly inhibited tumor growth compared to irinotecan only, indicating some potentiation of the anti-tumor effects of irinotecan by CA4P. A number of mechanisms may explain this enhanced activity when the two agents are combined. CA4 could induce changes in the tumor microenvironment that enhance the cell-killing activity of irinotecan. Our results showed that CA4 LONDs-MBs or CA4P caused a reduction in perfusion, potentially leading to the entrapment of irinotecan or its active metabolite SN38 in tumor tissue, thus prolonging the exposure times of tumor cells to the active agent. Trapping of cytotoxic agents by CA4P and in particular using irinotecan in combination with CA4P have been previously demonstrated.[59] A trapping effect was not observed in the present study as the biodistribution data at 1 h post-injection showed the highest concentrations of irinotecan, SN38 and SN38G in the irinotecan only group. However, these tissues were collected following five treatments; therefore, the tumor vasculature could potentially have already been significantly altered and thus hindered the entry of irinotecan as measured by this final time-point. Single treatments at multiple timings of irinotecan and CA4-LONDs-MBs administered would be required to investigate the trapping effect.

The potentiation effect shown with CA4 and irinotecan may also result from their different cell targets; thus, this regimen generates a multi-targeting strategy. Irinotecan acts on the most rapidly proliferating tumor cells, while in contrast, CA4 affects the established vasculature. This has been previously demonstrated with CA4P and 5-fluorouracil (5-FU), where 5-FU inhibited tumor cells in the viable rim[44]; in this case, no trapping was observed. Low dose irinotecan (10 mg/kg × 2 per week) has also been shown to suppress the mobilization of circulating endothelial progenitor cells (CEPs) in a murine colon cancer model.[60] CEPs are a known cause of resistance to CA4[61] treatment and could contribute to the enhanced anti-tumor activity seen here.

Taken together the data presented in this study suggest that LONDs are a promising hydrophobic drug delivery nanovehicle. Their use alone or attached to MBs suggests that this technology has the potential to enhance drug delivery of poorly water-soluble drugs while significantly reducing the need for high circulating concentrations. Furthermore, the combination of low dose irinotecan and CA4 holds great promise for effective cancer treatment.

Credit Author Statement

Conceptualization, methodology, formal analysis, investigation, data curation, visualization, writing - review & editing, resources: A.C., V.M, G.M., L.E.M., N.I., S.D.E, P.L.C. Methodology, investigation: A.W., M.V. Conceptualization and software: S.A.P., J.R.M. Conceptualization, supervision, funding acquisition: B.R.J., A.F.M., S.D.E., P.L.C.

Uncited references

Q19

62, 63

Appendix A. Supplementary data

Supplementary data to this article can be found online at https://doi.org/10.1016/j.nano.2021.102401.

References

1. Kalepu S, Nekkanti V. Insoluble drug delivery strategies: review of recent advances and business prospects. *Acta Pharm Sin B* 2015;**5**:442-453.
2. Chase DM, Chaplin DJ, Monk BJ. The development and use of vascular targeted therapy in ovarian cancer. *Gynecol Oncol* 2017;**145**:393-406.
3. El-Emir E, Boxer GM, Petrie IA, Boden RW, Dearling JLJ, Begent RHJ, et al. Tumour parameters affected by combretastatin A-4 phosphate therapy in a human colorectal xenograft model in nude mice. *Eur J Cancer* 2005;**41**:799-806.
4. Zhao D, Jiang L, Hahn EW, Mason RP. Tumor physiologic response to combretastatin A4 phosphate assessed by MRI. *Int J Radiat Oncol Biol Phys* 2005;**62**:872-880.
5. Seiler GS, Ziemer LS, Schultz S, Lee WMF, Sehgal CM. Dose-response relationship of ultrasound contrast agent in an in vivo murine melanoma model. *Cancer Imaging* 2007;**7**:216-223.
6. Tozer GM, Kanthou C, Baguley BC. Disrupting tumour blood vessels. *Nat Rev Cancer* 2005;**5**:423-435.
7. Pettit GR, Singh SB, Schmidt JM, Niven ML, Hamel E, Lin CM. Isolation, structure, synthesis, and antimitotic properties of combretastatins B-3 and B-4 from Combretum caffrum. *J Nat Prod* 1988;**51**:517-527.
8. Pettit GR, Singh SB, Hamel E, Lin CM, Alberts DS, Garcia-Kendal D. Isolation and structure of the strong cell growth and tubulin inhibitor combretastatin A-4. *Experientia* 1989;**45**:209-211.
9. Gaspari R, Prota AE, Bargsten K, Cavalli A, Steinmetz MO. Structural basis of cis- and trans-combretastatin binding to tubulin. *Chem* 2017;**2**:102-113.
10. Chaplin DJ, Pettit GR, Hill SA. Anti-vascular approaches to solid tumour therapy: evaluation of combretastatin A4 phosphate. *Br J Cancer* 1996;**74**:S86-S88.
11. Grosios K, Holwell SE, McGown AT, Pettit GR, Bibby MC. In vivo and in vitro evaluation of combretastatin A-4 and its sodium phosphate prodrug. *Br J Cancer* 1999;**81**:1318-1327.
12. Pettit GR, Singh SB, Boyd MR, Hamel E, Pettit RK, Schmidt JM, et al. Antineoplastic agents .291. Isolation and synthesis of combretastatin A-4, A-5 and A-6. J Med Chem 1995;38:1666–72.
13. Cooney MM, Radivoyevitch T, Dowlati A, Overmoyer B, Levitan N, Robertson K, et al. Cardiovascular safety profile of combretastatin A4 phosphate in a single-dose phase I study in patients with advanced cancer. *Clin Cancer Res* 2004;**10**:96-100.
14. Mooney CJ, Nagaiah G, Fu P, Wasman JK, Cooney MM, Savvides PS, et al. A phase II trial of fosbretabulin in advanced anaplastic thyroid carcinoma and correlation of baseline serum-soluble intracellular adhesion molecule-1 with outcome. *Thyroid* 2009;**19**:233-240.
15. Jiang H, Li ZP, Tian GX, Pan RY, Xu CM, Zhang B, et al. Liver-targeted liposomes for codelivery of curcumin and combretastatin A4 phosphate: preparation, characterization, and antitumor effects. *Int J Nanomedicine* 2019;**14**:1789-1804.
16. Wang J, Mongayt D, Torchilin VP. Polymeric micelles for delivery of poorly soluble drugs: preparation and anticancer activity in vitro of paclitaxel incorporated into mixed micelles based on poly(ethylene glycol)-lipid conjugated and positively charged lipids. *J Drug Target* 2005;**13**:73-80.

UNCORRECTED PROOF

ARTICLE IN PRESS

17. Fang JY, Hung CF, Hua SC, Hwang TL. Acoustically active perfluorocarbon nanoemulsions as drug delivery carriers for camptothecin: drug release and cytotoxicity against cancer cells. *Ultrasonics* 2009;**49**:39-46.
18. Chen T, Gong T, Zhao T, Fu Y, Zhang Z, Gong T. A comparison study between lycobetaine-loaded nanoemulsion and liposome using nRGD as therapeutic adjuvant for lung cancer therapy. *Eur J Pharm Sci* 2018;**111**:293-302.
19. Bertrand N, Wu J, Xu X, Kamaly N, Farokhzad OC. Cancer nanotechnology: the impact of passive and active targeting in the era of modern cancer biology. *Adv Drug Deliv Rev* 2014;**66**:2-25.
20. Sindhwani S, Syed AM, Ngai J, Kingston BR, Maiorino L, Rothschild J, et al. The entry of nanoparticles into solid tumours. *Nat Mater* 2020;**19**:566-575.
21. Kotopoulis S, Dimcevski G, Gilja OH, Hoem D, Postema M. Treatment of human pancreatic cancer using combined ultrasound, microbubbles, and gemcitabine: a clinical case study. Med Phys 2013;40:072902–1–072902–9.
22. Lentacker I, De Smedt SC, Sanders NN. Drug loaded microbubble design for ultrasound triggered delivery. *Soft Matter* 2009;**5**:2161-2170.
23. Willmann JK, Bonomo L, Testa AC, Rinaldi P, Rindi G, Valluru KS, et al. Ultrasound molecular imaging with BR55 in patients with breast & ovarian lesions: first-in-human results. *J Clin Oncol* 2017;**35**:2133-2140.
24. Tartis MS, McCallan J, Lum AFH, LaBell R, Stieger SM, Matsunaga TO, et al. Therapeutic effects of paclitaxel-containing ultrasound contrast agents. *Ultrasound Med Biol* 2006;**32**:1771-1780.
25. Villanueva FS, Jankowski RJ, Klibanov S, Pina ML, Alber SM, Watkins SC, et al. Microbubbles targeted to intercellular adhesion molecule-1 bind to activated coronary artery endothelial cells. *Circulation* 1998;**98**:1-5.
26. Ingram N, Mcveigh LE, Abou-saleh RH, Maynard J, Peyman SA, McLaughlan JR, et al. Ultrasound-triggered therapeutic microbubbles enhance the efficacy of cytotoxic drugs by increasing circulation and tumor drug accumulation and limiting bioavailability and toxicity in normal tissues. *Theranostics* 2020;**10**:10973-10992.
27. Lentacker I, De Cock I, Deckers R, De Smedt SC, Moonen CTW. Understanding ultrasound induced sonoporation: definitions and underlying mechanisms. *Adv Drug Deliv Rev* 2014;**72**:49-64.
28. Mico V, Charalambous A, Peyman SA, Abou-Saleh RH, Markham AF, Coletta PL, et al. Evaluation of lipid-stabilised tripropionin nanodroplets as a delivery route for combretastatin A4. *Int J Pharm* 2017;**526**:547-555.
29. National Center for Biotechnology Information. Glyceryl tripropanoate. PubChem Compd Database 2005. , https://pubchem.ncbi.nlm.nih.gov (accessed April 24, 2018).
30. Peyman SA, Abou-Saleh RH, McLaughlan JR, Ingram N, Johnson BRG, Critchley K, et al. Expanding 3D geometry for enhanced on-chip microbubble production and single step formation of liposome modified microbubbles. Lab Chip 2012;12:4544–4522.
31. Mico V. *Developing microbubble-nanodroplet composites for enhanced hydrophobic drug delivery*; 2017.
32. Abdelrahman MA, Marston G, Hull MA, Markham AF, Jones PF, Evans JA, et al. High-frequency ultrasound for in vivo measurement of colon wall thickness in mice. *Ultrasound Med Biol* 2012;**38**:432-442.
33. McVeigh LE, Wijetunga I, Ingram N, Marston G, Prasad R, Markham AF, et al. Development of orthotopic tumour models using ultrasound-guided intrahepatic injection. *Sci Rep* 2019;**9**:1-9.
34. Cullis ER, Kalber TL, Ashton SE, Cartwright JE, Griffiths JR, Ryan AJ, et al. Tumour overexpression of inducible nitric oxide synthase (iNOS) increases angiogenesis and may modulate the anti-tumour effects of the vascular disrupting agent ZD6126. *Microvasc Res* 2006;**71**:76-84.
35. Kalra AV, Kim J, Klinz SG, Paz N, Cain J, Drummond DC, et al. Preclinical activity of nanoliposomal irinotecan is governed by tumor deposition and intratumor prodrug conversion. *Cancer Res* 2014;**74**:7003-7013.
36. Murata R, Overgaard J, Horsman MR. Comparative effects of combretastatin A-4 disodium phosphate and 5,6-dimethylxanthenone-4-acetic acid on blood perfusion in a murine tumour and normal tissues. *Int J Radiat Biol* 2001;**77**:195-204.
37. Dark GG, Hill SA, Prise VE, Tozer GM, Pettit GR, Chaplin DJ. Combretastatin A-4, an agent that displays potent and selective toxicity toward tumor vasculature. Cancer Res 1997;57:1829–34.
38. Chaplin DJ, Hill SA. The development of combretastatin A4 phosphate as a vascular targeting agent. *Int J Radiat Oncol Biol Phys* 2002;**54**:1491-1496.
39. Liang W, Ni Y, Chen F. Tumor resistance to vascular disrupting agents: mechanisms, imaging, and solutions. *Oncotarget* 2016;**7**:15444-15459.
40. Fioravanti A, Canu B, Alì G, Orlandi P, Allegrini G, Di Desidero T, et al. Metronomic 5-fluorouracil, oxaliplatin and irinotecan in colorectal cancer. *Eur J Pharmacol* 2009;**619**:8-14.
41. Hill SA, Chaplin DJ, Lewis G, Tozer GM. Schedule dependence of combretastatin A4 phosphate in transplanted and spontaneous tumour models. *Int J Cancer* 2002;**102**:70-74.
42. Kerbel RS, Kamen BA. The anti-angiogenic basis of metronomic chemotherapy. *Nat Rev Cancer* 2004;**4**:423-436.
43. Parkins CS, Holder a L, Hill SA, Chaplin DJ, Tozer GM. Determinants of anti-vascular action by combretastatin A-4 phosphate: role of nitric oxide. Br J Cancer 2000;83:811–6.
44. Grosios K, Loadman PM, Swaine DJ, Pettit GR, Bibby MC. Combination chemotherapy with combretastatin A-4 phosphate and 5-fluorouracil in an experimental murine colon adenocarcinoma. *Anticancer Res* 2000;**20**:229-234.
45. Vincent L, Kermani P, Young LM, Cheng J, Zhang F, Shido K, et al. Combretastatin A4 phosphate induces rapid regression of tumor neovessels and growth through interference with vascular endothelial-cadherin signaling. *J Clin Invest* 2005;**115**:2992-3006.
46. Siemann DW. The unique characteristics of tumor vasculature and preclinical evidence for its selective disruption by tumor-vascular disrupting agents. *Cancer Tretment Rev* 2011;**37**:63-74.
47. Escoffre JM, Novell A, Serrière S, Lecomte T, Bouakaz A. Irinotecan delivery by microbubble-assisted ultrasound: in vitro validation and a pilot preclinical study. *Mol Pharm* 2013;**10**:2667-2675.
48. Nallamothu R, Wood GC, Pattillo CB, Scott RC, Kiani MF, Moore BM, et al. A tumor vasculature targeted liposome delivery system for combretastatin A4: design, characterization, and in vitro evaluation. *AAPS PharmSciTech* 2006;**7**:E1-10.
49. Zhang Y, Wang J, Bian D, Zhang X, Zhang Q. Targeted delivery of RGD-modified liposomes encapsulating both combretastatin A-4 and doxorubicin for tumor therapy : in vitro and in vivo studies. *Eur J Pharm Biopharm* 2010;**74**:467-473.
50. Dai W, Jin W, Zhang J, Wang X, Wang J, Zhang X, et al. Spatiotemporally controlled co-delivery of anti-vasculature agent and cytotoxic drug by octreotide-modified stealth liposomes. *Pharm Res* 2012;**29**:2902-2911.
51. Su T, Long Y, Deng C, Feng L, Zhang X, Chen Z, et al. Construction of a two-in-one liposomal system (TWOLips) for tumor-targeted combination therapy. *Int J Pharm* 2014;**476**:241-252.
52. Nallamothu R, Wood GC, Kiani MF, Moore BM, Horton FP, Thoma LA. A targeted liposome delivery system for combretastatin A4: formulation optimization through drug loading and in vitro release studies. *PDA J Pharm Sci Technol* 2006;**60**:144-155.
53. Wang Y, Chen H, Liu Y, Wu J, Zhou P, Wang Y, et al. pH-sensitive pullulan-based nanoparticle carrier of methotrexate and combretastatin A4 for the combination therapy against hepatocellular carcinoma. *Biomaterials* 2013;**34**:7181-7190.
54. Malcontenti-Wilson C, Muralidharan V, Skinner S, Christophi C, Sherris D, O'Brien PE. Combretastatin A4 prodrug study of effect on the growth and the microvasculature of colorectal liver metastases in a murine model. *Clin Cancer Res* 2001;**7**:1052-1060.
55. Nabha SM, Mohammad RM, Wall NR, Dutcher JA, Salkini BM, Pettit GR, et al. Evaluation of combretastatin A-4 prodrug in a non-Hodgkin's

UNCORRECTED PROOF

ARTICLE IN PRESS

lymphoma xenograft model: preclinical efficacy. *Anticancer Drugs* 2001;**12**:57-63.
56. Salmon BA, Siemann DW. Characterizing the tumor response to treatment with combretastatin A4 phosphate. *Int J Radiat Oncol Biol Phys* 2007;**68**:211-217.
57. Zhang P, Chen Y, Liu JF, Yang Y, Lv Q, Wang J, et al. Quantitative evaluation of combretastatin A4 phosphate early efficacy in a tumor model with dynamic contrast-enhanced ultrasound. *Ultrasound Med Biol* 2018;**44**:840-852.
58. Nguyen L, Fifis T, Malcontenti-Wilson C, Chan LS, Costa PNL, Nikfarjam M, et al. Spatial morphological and molecular differences within solid tumors may contribute to the failure of vascular disruptive agent treatments. *BMC Cancer* 2012;**12**:1-13.
59. Wildiers H, Ahmed B, Guetens G, De Boeck G, de Bruijn EA, Landuyt W, et al. Combretastatin A-4 phosphate enhances CPT-11 activity independently of the administration sequence. *Eur J Cancer* 2004;**40**:284-290.
60. Murakami H, Ogata Y, Akagi Y, Ishibashi N, Shirouzu K. Circulating endothelial progenitor cells in metronomic chemotherapy using irinotecan and/or bevacizumab for colon carcinoma: study of their clinical significance. *Exp Ther Med* 2011;**2**:595-600.
61. Nathan P, Zweifel M, Padhani AR, Koh DM, Ng M, Collins DJ, et al. Phase I trial of combretastatin A4 phosphate (CA4P) in combination with bevacizumab in patients with advanced cancer. *Clin Cancer Res* 2012;**18**:3428-3439.
62. Abou-Saleh RH, Peyman SA, Johnson BRG, Marston G, Ingram N, Bushby R, et al. The influence of intercalating perfluorohexane into lipid shells on nano and microbubble stability. *Soft Matter* 2016;**12**:7223-7230.
63. Ingram N, Macnab SA, Marston G, Scott N, Carr IM, Markham AF, et al. The use of high-frequency ultrasound imaging and biofluorescence for in vivo evaluation of gene therapy vectors. *BMC Med Imaging* 2013;**13**:35.

UNCORRECTED PROOF

Q20 Supplementary material

AUTHOR QUERY FORM

ELSEVIER	**Journal: NANO** **Article Number: 102401**	**Please e-mail your responses and any corrections to:** **E-mail: Corrections_ESCH.elsevier@spi-global.com**

Dear Author,

Please check your proof carefully and mark all corrections at the appropriate place in the proof (e.g., by using on-screen annotation in the PDF file) or compile them in a separate list. Note: if you opt to annotate the file with software other than Adobe Reader then please also highlight the appropriate place in the PDF file. To ensure fast publication of your paper please return your corrections within 48 hours.

For correction or revision of any artwork, please consult http://www.elsevier.com/artworkinstructions.

We were unable to process your file(s) fully electronically and have proceeded by

☐ Scanning (parts of) your article ☐ Rekeying (parts of) your article ☐ Scanning the artwork

Any queries or remarks that have arisen during the processing of your manuscript are listed below and highlighted by flags in the proof. Click on the 'Q' link to go to the location in the proof.

Location in article	Query / Remark: click on the Q link to go Please insert your reply or correction at the corresponding line in the proof
Q1	Your article is registered as a regular item and is being processed for inclusion in a regular issue of the journal. If this is NOT correct and your article belongs to a Special Issue/Collection please contact j.m.francis@elsevier.com immediately prior to returning your corrections.
Q2	The author names have been tagged as given names and surnames (surnames are highlighted in teal color). Please confirm if they have been identified correctly.
Q3, Q5, Q6, Q7, Q8, Q9, Q10, Q11, Q12, Q13, Q14, Q15, Q16, Q17	Professional Degree (e.i., PhD, MD, MSc, etc.) is mandatory for this journal. Please check and provide.
Q4	Please indicate each author's full given name and academic degree.
Q18	Please check this sentence for clarity.
Q19	Uncited references: This section comprises references that occur in the reference list but not in the body of the text. Please position each reference in the text or, alternatively, delete it. Thank you.
Q20	Supplementary caption was not provided. Please check the suggested data if appropriate, and correct if necessary. Please check this box if you have no corrections to make to the PDF file. ☐

Thank you for your assistance.